Analytical Methods

ROYAL SOCIETY OF CHEMISTRY

PAPER

View Article Online
View Journal | View Issue

Cite this: *Anal. Methods*, 2025, **17**, 7692

Structural analysis of synthetic opioids using travelling wave ion mobility-mass spectrometry (TWIM-MS)†

Karen Abigail Reyes Monroy,[a] Daillin L. Perez,[a] Rebecca Demmelash,[a] Lilly T. Ngo,[a] Ariana M. Mancilla Rodriguez,[a] Haley A. Castro,[a] Noah R. Wiese,[b] Wilbert A. Murillo,[b] Dr. Teresa D. Golden[a] and Dr. Guido F. Verbeck *[b]

Traveling wave ion mobility-mass spectrometry (TWIM-MS) has emerged as a powerful tool for the identification of synthetic opioids, such as fentanyl and its analogs. However, due to its novelty, only a few fentanyl analogs have been studied using this technology and alternative drift gases, apart from the commonly employed nitrogen gas. Here we introduce the largest compendium of measured $^{TW}CCS_{N_2}$, $^{TW}CCS_{He}$, and $^{TW}CCS_{CO_2}$ values for fentanyl-related compounds. This compendium of mobility-derived CCS molecular descriptors for precursor $[M + H]^+$ ions can be used to assign fentanyl identities. Here, we report collision-cross section (CCS) values for precursor $[M + H]^+$ ions of 110 fentanyl analogs, 7 fentanyl precursors, and 31 non-fentanyl related synthetic opioids measured using three mobility gases; nitrogen, helium, and carbon dioxide. Measured $^{TW}CCS_{N_2}$ values show high agreement with previously published collision cross-section values obtained *via* drift-tube ion mobility (DTIM) MS, with differences ranging from −0.1 to 1.3%. Additionally, computationally derived CCS values for each fentanyl analyte were calculated using MobCross, with a difference range of ±3–15% between theoretical and experimental values.

Received 17th December 2024
Accepted 19th March 2025

DOI: 10.1039/d4ay02263g

rsc.li/methods

1. Introduction

Fentanyl is a synthetic opioid that belongs to a group of medicines called opioid analgesics and has made great strides in the medical field since its introduction into the pharmaceutical market as a pain management drug.[1,2] It was first synthesized by Janssen Pharmaceutica in the 1950s and it works by attaching to μ-receptors mainly in the brain, inducing feelings of euphoria and, at higher dosages, leading to analgesia or anesthesia.[3] Currently, low dosages of fentanyl and fentanyl analogs (remifentanil, alfentanil, and sufentanil) are commonly administered to provide pain relief during post-surgical procedures.[4] And while fentanyl has rightfully earned its place in medical settings, its misuse and widespread presence continue to severely damage several communities worldwide.[5–7] In the United States, deaths due to drug overdoses involving fentanyl and its analogs continue. Early in its introduction, the misuse of medically prescribed fentanyl was the primary cause for opioid overdoses leading to death in the U.S.[8,9] Studies have shown that repeated use of opioid painkillers often leads to dependence and abuse which increases the risk of a life-threatening overdose.[10,11] Such an increase in incidence of fentanyl overdoses led to tighter medical restrictions on the prescribed opioid drug. Fentanyl and fentanyl analogs used in medical settings are now classified as Schedule II controlled substances under the Controlled Substances Act (CSA).[12] Soon after this, a rise in clandestinely produced fentanyl in the black market was observed in the U.S.[13] In response, the drug enforcement administration (DEA) has placed several restrictions and closely monitors chemical reagents commonly used for the illicit production of fentanyl and fentanyl analogs.[14]

In the U.S. fentanyl overdose deaths mainly involve multiple drugs, such as cocaine and methamphetamine, which are popular recreational drugs.[12,15] Most recently law officials have reported an increase in the number of cases where illicit counterfeit pills, marketed as oxycodone or benzodiazepine medication, are found laced with small amounts of fentanyl and/or fentanyl analogs.[16–19] Drug lacing is often carried out by clandestine manufacturers to increase the desired effect of the product while decreasing production costs.[20,21] While the amounts of fentanyl and related drugs found in confiscated drugs are minimal (3–11%), the potency of fentanyl is known to be 100 times stronger than morphine and 50 times stronger than heroin, making it extremely dangerous for consumers.[17,22] Lethal does for humans are often as small as 2 milligrams.[17,22] Making matters worse, clandestine laboratories aren't known to

[a]*Department of Chemistry, University of North Texas, Denton, TX, USA*
[b]*Department of Chemistry and Biochemistry, Augusta University, Augusta, GA, USA. E-mail: gverbeck@augusta.edu*

† Electronic supplementary information (ESI) available. See DOI: https://doi.org/10.1039/d4ay02263g

produce pure fentanyl.[23,24] In 2021, a study conducted by the Fentanyl Profiling Program (FPP) of the DEA analyzed 538 fentanyl and fentanyl-related samples and found fentanyl purity ranging from 0.2% to 36.4%, with an average purity of 13.6%.[25] Furthermore, 46 out of these samples contained both fentanyl and fentanyl analogs.[25] This is partly due to the numerous restrictions placed on fentanyl reagents. To circumvent regulations and detection, clandestine laboratories use reagents that are not highly regulated to produce fentanyl analogs that are structurally similar in their backbone but have different functional groups.[6,26,27] The issue with such practices is the drastically varying potencies of fentanyl analogs. For example, carfentanil used to sedate large mammals, such as elephants and bears, is 100 times more potent than fentanyl, whereas analogs such as acetylfentanyl and butyryl fentanyl are less potent.[28] This highlights the importance of correctly characterizing fentanyl analogs found in illicit drugs. In addition to identifying fentanyl analogs, correct characterization of these chemicals' sheds light on the synthetic routes followed for its production, which in turn aids drug enforcement officials in deciding which reagents require restrictions or further monitoring.[29]

Presently, 212 fentanyl analogs have been cataloged by companies such as Cayman Chemicals. Currently, forensic analytical protocols for illicit drug analysis require the implementation of two or more analytical techniques. The first test forensic scientists conduct is a presumptive test, also known as a screening test. This screening phase is conducted when an illegal component is presumed to be present in a substance. Some commonly used screening tests in forensic laboratories are immunoassays and the Marquis test. These tests are typically fast and only provide chemical class-selectivity, and no structurally specific data. Once the presence of the suspected entity is confirmed, the sample is sent for further analysis; this stage is known as the confirmatory phase. In accordance with guidelines set by ASTM International E2329-Standard Practice or the Scientific Working Group for the Analysis of Seized Drugs (SWGDRUG) recommendations, practitioners confirm the identity of a chemical entity using analytical methods that provide structural specificity, known as confirmatory tests.[30,31] These tests are divided into two categories, category A and B, and are implemented with the goal of providing structurally specific molecular descriptors that will aid in compound identification. Category B tests, which include several chromatographic techniques, provide chemical and physical selectivity, while category A tests, such as IR, NMR, XRD and MS, provide structure-specific information.[32,33] To comply with forensic guidelines, practitioners must (a) implement two analytical techniques, one of which must be from category A, and the other from category A, B, or C, of which screening tests are a part of, or (b) use two category B techniques in addition to one other category B or C technique. Currently, gas-chromatography-electron ionization-mass spectrometry (GC-EI-MS) is the gold standard analytical tool used for the detection and characterization of fentanyl-related substances.[34]

There are several benefits of using GC-EI-MS, such as low sample volume requirements, low detection limits, and high structural specificity. Furthermore, chromatographic and mass spectral data are obtained, providing two useful structural molecular descriptors. However, several challenges with the implementation of GC-MS for fentanyl characterization have arisen over the years.[35] Electron ionization is a hard ionization technique known to generate a large number of ionized fragments, while providing very little or no data regarding the intact molecular ion. While fingerprint data for analytes of interest are valuable and often required, the lack of precursor ion data is making it increasingly difficult for forensic scientists to assign structural identity to fentanyl analogs that fragment similarly. As mentioned earlier, fentanyl analogs are structurally similar entities. Their core structure remains the same, but the attached functional groups can differ very drastically.[36,37] The fragmentation patterns of these analogs differ depending on the ionization method, but in the case of EI, several fentanyl moieties produce EI-MS spectrums that are very similar.[38,39] While several optimization efforts can be made on the GC side, very little can be done to control the fragmentation preference of the analog during EI.[40] One approach to combat this is to compare the intensities of the fragments. While this can provide some additional confidence in the identification processes, it is not the suggested method when comparing spectrum data where intensities do not differ drastically.[41,42] In such instances practitioners might wish to implement another category A technique, such as ESI-MS for further confirmation.[41,43–47] Electrospray ionization (ESI) is a soft-ionization technique that produces intact molecular species for analysis. Controlled CID of these ions can provide extremely useful fingerprint data for fentanyl identification. Liquid chromatography can be used in conjunction with ESI-MS to provide retention time and MS data for fentanyl characterization.[48,49] While LC provides an additional layer of separation, some fentanyl isomers require specially manufactured columns that provide sufficient separation for confident identification, making such chromatographic methods costly in addition to being time-consuming. This situation is not ideal as current challenges in illicit drug identification are driving practitioners to search for analytical techniques that provide several structural molecular descriptors in a timely and cost-efficient manner.

A relatively new analytical technique known as ion mobility-mass spectrometry (IM-MS) has emerged as a powerful tool for the identification of drugs in forensic and security applications. Since its introduction, several types of IM methods have emerged. Traditionally, the field has been dominated by drift tube-ion mobility (DTIM), yet other methods, such as Traveling Wave Ion Mobility (TWIM) show promise as contenders.[50,51] TWIM CCS measurements are performed when a charged ion traverses a mobility cell under oscillating electric fields, in contrast to the uniform electric field used to pull ions through in DTIM.[52,53] Within the electric field, ions are separated based on size, shape and charge. For example, larger and more complex molecules with greater surface areas provide a larger target for collisions compared to smaller and more compact molecules; therefore, these larger mobility gases will generally exhibit larger CCS values.[52,54] Additionally, when a charged ion,

such as a positively charged $[M + H]^+$ fentanyl analog precursor ion, moves through a mobility cell it can induce a temporary dipole moment in neutral gas molecules like carbon dioxide.[54,55] This occurs because the electric field of the charged ion polarizes the neutral molecule, distorting its electron cloud.[54,55] The strength of this dipole-induced interaction depends on the polarizability of the neutral molecule and its proximity to the ion. For a molecule like CO_2, which is non-polar in its neutral state, its electrons can be distorted by the ion's electric field, creating a weak dipole.[54–56] These interactions cause an ion to experience attractive or repulsive forces depending on the orientation of the induced dipoles, which can slow its drift resulting in a larger CCS.[54–56] For example, less polarizable gases like nitrogen or helium induce weaker dipole interactions than carbon dioxide, resulting in smaller drift times and CCS values.[54–56] Temperature and velocity also alter the collision dynamics of an ion–neutral interaction.[54–56] Faster molecules at higher temperatures and slower molecules at lower temperatures alter the type of elastic or inelastic collisions, resulting in varying CCS values.[54–56]

Lastly, the extent of energy transfer during collisions, influenced by internal degrees of freedom (such as vibrations), can modify the measured CCS, as well.[54–56] These are some of the main interactions that are considered when calculating accurate drift times for ions. Furthermore, unlike LC retention times, mobility (K_0) and CCS values are physical molecular properties and are thus highly reproducible and robust if determined with high accuracy and precision.[57–59] Here, we aim to contribute to the existing CCS compendium currently present for fentanyl and fentanyl analogs. Most recently, Hollerbach *et al.* and Aderorho *et al.* both obtained CCS values for fentanyl protomers using ion mobility mass spectrometry.[60,61] Johnson *et al.* demonstrated how the ratio of protomer intensity could vary with solvent conditions, while Aderoho *et al.* demonstrated how ion mobility separation of fentanyl isomers could be improved using metal cation adducts.[62,63] Forero *et al.* used trapped ion mobility to develop a fast high-throughput method for the screening of 185 fentanyl analogs, while also providing CCS data for product ions.[64]

In this study we conduct ESI-TWIM-MS analysis, using the Synapt G2-Si HDMS by Waters, to measure the nitrogen, helium, and carbon dioxide CCS values of 148 synthetic opioids, of which 110 are fentanyl analogs, 7 are fentanyl precursors, intermediates, and impurities, and 31 are non-fentanyl synthetic opioids. CCS measurements have traditionally been performed using helium as the drift gas, but as IM instrumentation became commercialized, nitrogen has become another popular choice due to its cost, availability and generally better resolving power.[65] According to May *et al.* both CCS_{He} and CCS_{N_2} values account for the vast majority of CCS values reported in literature, with CCS_{N_2} values being slightly more prevalent, while only 5% of the reported values account for other gases.[65] Only a handful of studies have reported working with alternative drift gases such as carbon dioxide, which accounts for 0.3% of the values reported.[65] Furthermore, to the best of our knowledge only $^{DT}IM_{N_2}$ measurements have been performed for only a handful of fentanyl analogs which we will discuss here. We use these existing values to test the accuracy of our obtained CCS values. May and co-authors also reported that only 9% of CCS values reported were obtained using TWIMS; thus we aim to increase this number through this publication.[65] Measured $^{TW}CCS_{N_2}$, $^{TW}CCS_{He}$, and $^{TW}CCS_{CO_2}$ values alongside accurate-mass values were used to build the largest ^{TW}CCS database known to date for fentanyl analogs. Theoretical CCS measurements were also performed for each experimentally obtained precursor ion $[M + H]^+$ using MobCross, a program that predicts ion cross-sections by utilizing both established and derived equations, along with Monte Carlo simulations.[66] We have compiled these molecular descriptors with the expectation that they will complement chromatographic, mass spectral, and fragmentation data in supporting fentanyl analog identification.

2. Experimental

2.1 Chemicals and reagents

Optima™ LC-MS grade methanol, acetonitrile, and water were purchased from Fisher Scientific (Pittsburg, USA). Acetic acid 99.99% (Sigma-Aldrich, USA) and sodium hydroxide (Fisher-Scientific, USA) were also purchased. A Major Mix IMS/TOF Calibration Kit [186008113] and leucine-enkephalin [186008113] solution, both purchased from Waters (MA, USA), were used for CCS calibration and as a lock mass solution.

A total of 148 synthetic opioid standards from the Fentanyl Analogue Screening Kit (FASK) – 1 & 2 and emergent panels 3 and 4, with molecular weights ranging from 99 to 536 g mol^{-1}, were obtained from Cayman Chemicals (Ann Arbor, MI, USA). Please refer to Table S5† for a list of opioid standards used and their Cayman ID numbers, molecular formula and molecular mass. The standards were shipped in powder form (0.2 mg sample per Eppendorf) were reconstituted in 200 μL of Optima™ LC-MS grade methanol (Fisher Scientific) to create stock solutions with 1 mg mL^{-1} concentration. To ensure homogeneity, stock solutions were vortexed at 650 rpm for 15 minutes prior to sample preparation. 1 ppm sample solutions for positive mode analysis were prepared by adding 1 μL of stock solution to a 999 μL of Optima™ LC-MS grade methanol containing 0.1% acetic acid (v/v).

The IM sector of the instrument was calibrated using Major Mix IMS/ToF Calibration Kit solution, which was prepared and used as specified by the manufacturer. A 0.5 M sodium formate solution in 1 : 1 (v/v) water : isopropanol was prepared using 99.9% pure sodium hydroxide purchased from Fisher Scientific (Pittsburg, USA) and used for mass calibration of the time-of-flight tube analyzer of the mass spectrometer. The mass calibrant solution contained sodium formate ions with m/z values ranging from 50 to 1200 in positive-ion mode.

2.2 Instrumentation

Three independent ESI-TWIM-MS experiments, using high purity nitrogen, helium, and carbon dioxide separately as ion mobility drift gas, were conducted on a Synapt G2-Si HDMS (Waters Corp., Milford, MA) equipped with an electrospray

ionization (ESI) source. A syringe pump was used to infuse samples at a flow rate of 3 μL mL^{-1} into the ESI source without prior LC column separation. The ESI source temperature was set to 80 °C and operated in positive ion mode (ESI+) with a 3 kV voltage, 20 V cone voltage, and a 50 V source offset voltage. Stable spray conditions were achieved by using nitrogen auxiliary gases with a set cone gas flow rate of 30 L h^{-1}, a desolvation gas flow rate of 600 L h^{-1} at 150 °C, and a nebulizer gas pressure of 6.5 bar.

2.3 Acquisition mode

A 3-minute run sequence was created and used to obtain mass-to-charge (m/z) and drift-time (DT) values for precursor ions $[M + H]^+$. Data were acquired in continuum mode at a scan rate of 500 ms for a total time of 3 minutes with the LockSpray function enabled. During the initial 30 seconds of the run sequence, a m/z range from 30 to 600 was scanned in resolution mode using the TOF HD-MS acquisition mode. Following this period, the acquisition mode was set to switch to the High Definition® MRM (HD-MRM) acquisition mode for the remaining run sequence time (2.5 minutes). Throughout the 2.5-minute scan the trap voltage was increased by 10 V every 30 seconds, thus providing MS/MS data obtained using trap voltages of 10, 20, 30, 40, and 50 V. The LockSpray reference, leucine enkephalin (200 pg μL^{-1}, 556.2771 Da), was used for single point mass correction across all three gas experiments, and for single point mobility correction in the nitrogen and helium mobility experiment, only.

2.4 TWIM parameters

The gas flow rates for the TriWave sector in all mobility gas experiments were as follows: trap cell (2 mL min^{-1}), IM cell (90 mL min^{-1}), and transfer cell (180 mL min^{-1}). It should be noted that since the instrument's internal IM cell mass flow controller (MFC) is calibrated only for nitrogen, a mass flow correction factor must be used to calculate the input flow rate for He and CO_2 in the IMS to maintain the required 1 bar IM cell pressure. Therefore, the desired relative N_2 flow rate (90 mL min^{-1}) and mass flow correction factors of 1.41 and 0.74 were used to calculate the input flow rates for He and CO_2, respectively. For a table of the gas flow rates used in each experiment, please refer to Tables S.2–S.4 of the ESI.† The ion mobility parameters for the nitrogen mobility gas experiment were as follows: default values for the trap region, a traveling wave velocity of 900 m s^{-1} with a height of 40 V for the IM sector, and a traveling wave velocity of 220 m s^{-1} with a height of 4 V for the transfer region. For CO_2 and He IM parameters, see Tables S.2–S.4 of the ESI.† The TOF mass analyzer was set to mass resolution mode ($m/\Delta m = 40\,000$) with a 0.5 seconds scan time.

2.5 Travelling-wave ion mobility CCS ($^{TW}CCS_{N_2}$, $^{TW}CCS_{He}$, and $^{TW}CCS_{CO_2}$) calibration

TWIM separates ions using oscillating DC waves in a gas filled stacked-ring ion guide (SRIG) with radial RF confinement. And due to the complex nature of these electric fields, CCS values cannot be directly calculated using the Mason–Schamp equation. Instead, these values are generally obtained by calibrating the instrument with calibrant ions possessing well-known DTIM CCS values (^{DT}CCS) and finding an empirically determined power-law relationship between the CCS values and ion drift times (t_d). Prior to data-acquisition, the Synapt G2-Si was switched to mobility mode and allowed to equilibrate for 1 hour. Once IM parameters were optimized for the experiment, the IM sector of the instrument was automatically calibrated using ^{DT}CCS reference data listed in Tables 1 and 2, using MassLynx V4.1 (Waters, Milford, MA, USA).

Table 1 Reference drift tube CCS values (Ω_{N_2}) for Major Mix IMS/TOF Calibration Kit [186008113] solution used as mobility calibrants in the present study for TWIM experiments using nitrogen as the mobility gas (Bush *et al.* 2012)[67]

Calibrant		$[M + H]^+$	CCS Ω_{N_2} [Å^2]
Acetaminophen	($n = 1$)	152.0711	130.4
Caffeine	($n = 1$)	195.0882	138.2
Sulfaguanidine	($n = 1$)	215.0602	146.8
Sulfadimethoxine	($n = 1$)	311.0814	168.4
Val–Tyr–Val	($n = 1$)	380.2185	191.7
Verapamil	($n = 1$)	455.2909	208.8
Terfenadine	($n = 1$)	472.3215	228.7
Polyalanine	($n = 1$)	516.2781	211.0
Leucine-enkephalin	($n = 11$)	556.2771	229.8
Polyalanine	($n = 1$)	587.3153	228.0
Reserpine	($n = 13$)	609.2812	252.3

Freshly prepared MajorMixQToF solution (50 μg mL^{-1}) containing polyalanine oligomers from $n = 3$ to $n = 14$ was used as the calibration mix. The calibrant ions had a mass range from 152 to 1921 Da and a ^{DT}CCS range extending from 130 to 373 Å^2. It should be noted that identical TWIMS parameters were used for both calibration and sample analysis. The calibrant solution covers a wide range of CCS values but the scope of this experiment only required calibrants with a max CCS value of 229.8 Å^2 to be analyzed.

$$t_c = t_d - \frac{C_{EDC}}{1000}\sqrt{\frac{m}{z}} \quad (1)$$

Therefore, only IMS calibrant ions within the mass range of 152 to 556 Da and the CCS range of 130 to 230 Å^2 were used. During calibration, the software measures and corrects the drift-times (t_d) for ions using eqn (1), which uses an instrument

Table 2 Reference drift tube CCS values (Ω_{He} and Ω_{CO_2}) for polyalanine oligomers used as mobility calibrants in the present study for TWIM experiments using helium and carbon dioxide as the mobility gases (Bush *et al.* 2012)[67]

Calibrant	$[M + H]^+$	CCS Ω_{He} [Å^2]	CCS Ω_{CO_2} [Å^2]
Polyalanine ($n = 3$)	232.12183	89	210.5
Polyalanine ($n = 4$)	303.15894	100	224.6
Polyalanine ($n = 5$)	374.19605	114	237.4
Polyalanine ($n = 6$)	445.23316	128	249.7
Polyalanine ($n = 7$)	516.27027	141	266.8
Polyalanine ($n = 8$)	587.30738	157	284.7

specific offset value known as the 'EDC delay coefficient' (1.45 for the Synapt G2-Si), to produce 'corrected drift-time' (t_c) values. Next, using eqn (2), normalized CCS (Ω_c) values of the calibrant ions are obtained by adjusting reference ^{DT}CCS values using reduced mass (μ) and its charge state (z).

$$\Omega_c = \frac{\sqrt{\mu}\Omega_d}{z} \quad (2)$$

The normalized collision cross section (Ω_c) values *vs.* corrected drift time (t_c) values of the calibrant ions were then plotted using a power regression model, which produces eqn (3) as the power trendline format. Calibration coefficients a and t_0, and exponent b were given in an output file. During automated CCS measurements, the analysis software (DriftScope V 1.2) uses the derived calibration coefficients to calculate experimental ^{TW}CCS values from measured drift times (t_d). The data used to plot the calibration curve as well as the calibration coefficients are shown in the ESI.†

$$\Omega_c = a(t_c + t_0)^b \quad (3)$$

For each independent mobility gas (N_2, He, and CO_2) experiment, ion mobility separation optimization and calibration were conducted as stated above. The calibration reference values and results for each experiment can be found in Fig. S.1 in the ESI.† Sample analysis commenced after successful IMS calibration and mass calibration.

2.6 TWIM analysis and data processing

All measurements were performed in triplicate. Inter-day data were obtained by performing data acquisitions per sample, with trials conducted within span of a week span. Data acquisition was performed using MassLynx (v4.1). HDMS^E data processing was performed using DriftScope (v2.0) to determine measured CCS values and to obtain arrival time distribution (ATD) plots. Here, the drift time data to CCS values were automatically converted using the calibration coefficients automatically generated by the software.

2.7 Theoretical CCS values

In the present study, we computationally determined CCS_{N_2} for the 110 fentanyl analogs analyzed using TWIM. First, neutral singlet structures for these compounds were created using Avogadro (v1.2.0) and optimized using molecular mechanics (MM) with the MMFF94 force field, 5000 steps, a steepest descent algorithm, and a convergence threshold of 10×10^{-8}. The optimization was continually performed until the energy of the molecule no longer changed. The MM-optimized geometries generated by Avogadro were saved as .xyz files and used as inputs for CCS calculations. CCS calculations were performed using MobCross which uses a quaternion algorithm to measure CCS values using Gaussian 98® coordinates from a .log output file and Cartesian coordinate files from Cerius®.[66] The program uses a projection approximation to estimate the collision cross-section of a gas-phase ion, derived from molecular mechanics calculations.

3. Results and discussion

3.1 Measured CCS

The ^{TW}CCS values were measured in triplicates and were highly reproducible, with the majority of (≥90%) ^{TW}CCS values for precursor ions $[M + H]^+$ having interday relative standard deviations (RSDs) less than 0.90%, 1.50%, and 0.50%, for N_2, He, and CO_2 mobility experiments, respectively. Table 3 lists TWIM-measured Ω_{N_2}, Ω_{He}, and Ω_{CO_2} values along with associated relative standard deviations (RSD) for 10 out of the 148 synthetic opioids, of which 110 are fentanyl analogs, 7 are precursors, intermediates, and impurities, and the remaining 31 are synthetic opioids from various classes. To see the full list please refer to Tables S.5–S.7 of the ESI.† It should be noted that CCS_{CO_2} values for 4-anilinopiperidine ($C_{11}H_{16}N_2$), were not successfully determined due to low peak intensity ($<1 \times 10^3$ counts).

$^{TW}CCS_{N_2}$ values for singly protonated $[M + H]^+$ species ranged from 139–220 Å^2 with inter-day standard deviation values ≤1.29%. The measured $^{TW}\Omega_{He}$ and $^{TW}\Omega_{CO_2}$ values ranged from 66–143 Å^2 and 179–268 Å^2, respectively with inter-day standard deviation values ≤2.90% and 0.75%. As depicted in Fig. 1, the ^{TW}CCS values for all 148 opioids were plotted against their mass-to-charge ratios (m/z) to illustrate the correlation between the two molecular descriptors in various mobility gases. As observed $^{TW}CCS_{N_2}$ values are systematically larger than $^{TW}CCS^{He}$ values and smaller than $^{TW}CCS_{CO_2}$ values. This is due

Table 3 Experimentally determined $^{TW}\Omega_{N_2}$, $^{TW}\Omega_{He}$, and $^{TW}\Omega_{CO_2}$ values for 10 fentanyl analogs. Values in parentheses are the relative standard deviation for the three IM measurements averaged to obtain the final CCS values

Fentanyl analog	$[M + H]^+$	Ω_{N_2} [Å^2]	Ω_{He} [Å^2]	Ω_{CO_2} [Å^2]
N-Methyl norfentanyl	247.18	158.78 (0.29)	86.68 (1.50)	199.69 (0.15)
Furanyl norfentanyl	271.144	163.41 (0.27)	92.49 (2.49)	212.52 (0.18)
Fentanyl	337.23	183.73 (0.56)	109.49 (1.34)	228.94 (0.21)
Para-methoxy acetyl fentanyl	353.22	189.23 (0.65)	113.94 (0.28)	235.61 (0.10)
Meta-methyl cyclopropyl fentanyl	363.24	193.91 (0.37)	116.12 (0.92)	237.85 (0.11)
Para-methyl butyryl fentanyl	365.26	194.48 (0.59)	114.25 (1.69)	239.01 (0.19)
Para-methoxy butyryl fentanyl	381.25	198.08 (0.56)	121.55 (0.29)	245.12 (0.10)
Para-methyl cyclopentyl fentanyl	391.27	200.32 (0.64)	122.52 (1.00)	246.26 (0.13)
N-(DOI) fentanyl	537.16	210.84 (0.37)	139.10 (2.58)	257.20 (0.52)
N-(DOBU) fentanyl	467.33	220.45 (0.94)	138.57 (0.38)	268.90 (0.16)

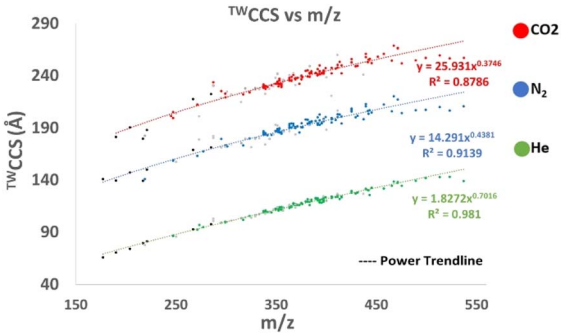

Fig. 1 CCS *versus m/z* plots for 148 synthetic opioids analyzed using three different mobility gases (CO_2, N_2, and He). 110 of these opioids are fentanyl analogs, 7 are fentanyl related opioids (black points), and 31 are non-fentanyl related opioids (grey points).

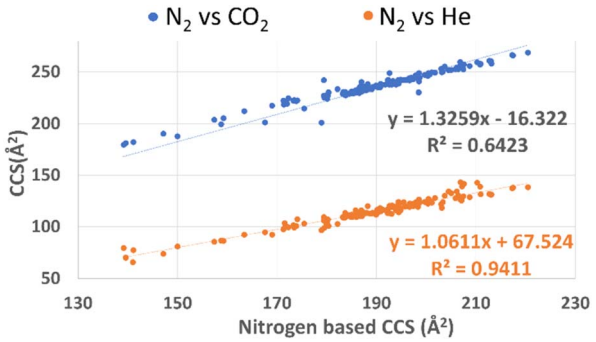

Fig. 2 Correlation trend between CCS values obtained using N_2, He, and CO_2 drift gases. CCS_{He} (*y*-axis) and CCS_{CO_2} (*y*-axis) values were plotted against CCS_{N_2} values (*x*-axis).

to differences in the polarizability of the gases, van der Waals radii and other factors that have a significant effect on the ion–neutral interactions.

For $^{TW}IM_{N_2}$, most CCS data points are found within the 182–207 Ω region, which represents 70% of the measured values. For $^{TW}IM_{He}$ and $^{TW}IM_{CO_2}$, 70% of the data points are found within the 103–127 Ω and 230–260 Ω region, respectively. As depicted in Fig. 1, fentanyl related compounds, such as precursors and impurities of fentanyl or its analogs, predominantly exhibit relatively small collision-cross sections (≤171 Ω_{N_2}, ≤98 Ω_{He}, and ≤222 Ω_{CO_2}). This is expected since such compounds are structurally smaller (177–285 *m/z*). Non-fentanyl opioids appear in the 141–207 Ω_{N_2}, 77–127 Ω_{He}, and 182–260 Ω_{CO_2} regions for $^{TW}IM_{N_2}$, $^{TW}IM_{He}$ and $^{TW}IM_{CO_2}$, respectively, and are not found in a distinct CCS region. Fig. 2 illustrates the correlation plots for nitrogen-based CCS values and the CCS values obtained using the remaining two gases (He and CO_2). Here we observe a relative change in CCS magnitude as the *m/z* of the analytes increases. As previously discussed, nitrogen is the standard drift gas employed in most commercialized IM instruments. Therefore, we chose to correlate $^{TW}CCS_{He}$ and $^{TW}CCS_{CO_2}$ values with $^{TW}IM_{N_2}$. As illustrated, the CCS values shift negatively by 16.3 and positively by 67.5 for CO_2 and He drift gases, respectively when compared to N_2. This drastic change can be attributed the distinct polarizability difference between helium (0.20×10^{-24} cm^3) and nitrogen (1.74×10^{-24} cm^3) which is more significant than the difference between carbon dioxide (2.91×10^{-24} cm^3) and nitrogen. As can be seen, the slope and intercept of the analytes differ, indicating varying interactions between the analyte ions and drift gas. This can be also attributed to the larger polarizability and size of CO_2 and N_2 gas molecules compared to He.

Table 4 Comparison between measured $^{TW}CCS_{N_2}$ values and previously published $^{DT}CCS_{N_2}$ values. Previously published values were assigned superscripts (a, b, or c)

Analyte	$[M + H]^+$ (*m/z*)	$^{TW}CCS_{N_2}$ (Å^2)	$^{DT}CCS_{N_2}$ (Å^2)	% difference ($^{TW}CCS_{N_2}$:$^{DT}CCS_{N_2}$)
Despropionyl *meta*-methylfentanyl	295.23	179.5	172.7 ± 0.1[a]	—
			179.4 ± 0.1[a]	0.1
(±)-*Cis*-isofentanyl	337.24	183.5	183.7 ± 0.1[a]	−0.1
			189.1 ± 0.1[a]	—
Fentanyl	337.26	183.7	184.1 ± 0.1[a]	−0.2
			189.1 ± 0.1[a]	—
Fentanyl	337.26	183.7	181.4 ± 0.1[b]	1.3
			—	—
Fentanyl	337.26	183.7	181.7 ± 0.1[c]	1.1
			187.9 ± 0.1[c]	—
Ortho-fluorofentanyl	355.23	184.6	184.7 ± 0.1[a]	−0.1
			190.5 ± 0.1[a]	—
Para-methyl acetyl fentanyl	337.24	186.0	186.4 ± 0.1[a]	−0.2
			—	—
Cyclopropyl fentanyl	349.24	187.1	186.2 ± 0.1[a]	0.5
			194.1 ± 0.1[a]	—
Isobutyryl fentanyl	351.24	187.8	187.4 ± 0.1[a]	0.3
			194.5 ± 0.1[a]	—
Butyryl fentanyl	351.27	188.2	188.3 ± 0.1[a]	−0.1
			194.9 ± 0.1[a]	—

[a] Nitrogen drift tube CCS values from Alderorho *et al.*, *Drug Test. Anal.*, 2024, **16**(4), 369–379. [b] Nitrogen drift tube CCS values from Lian *et al.*, *Anal. Methods*, 2018, **10**, 749–756. [c] Nitrogen drift tube CCS values from Butler *et al.*, *J. Am. Soc. Mass Spectrom.*, 2022, **33**, 1904–1913.

3.2 Comparing the obtained TWIM data with the published DTIM data

To validate the accuracy of our measured ^{TW}CCS values, we compared them with previously published ^{DT}CCS values. To our knowledge, the only published mobility data for some of the opioids analyzed in this study are from drift-tube ion mobility (DTIM) experiments conducted using nitrogen as the mobility gas. Therefore, only the published $^{DT}\Omega_{N_2}$ values are compared to our measured $^{TW}\Omega_{N_2}$ values to assess the accuracy of our CCS measurements. Thus, we would like to make it clear to the readers that the accuracy of $^{TW}\Omega_{N_2}$ will be based on the CCS values for the calibrant ions used. In a study conducted by Alderorho and colleagues, drift-tube ion mobility CCS ($^{DT}CCS_{N_2}$) values were obtained for fentanyl and 16 fentanyl analogs, of which 8 were also analyzed in this study.[68] As noted in Table 4, Alderorho *et al.* reported two DTCCS values for 7 out of these 8 compounds. These CCS values correspond to measurements for two protonation site isomers, referred to as 'protomers' of fentanyl analogs.[68] In our TWIM method, we do not see a second mobility peak for our analyzed $[M + H]^+$ *m/z* peaks. In Fig. 3, we present five fentanyl analogs *ortho*-methoxy butyryl fentanyl, senecioylfentanyl, *N*-(DOET) fentanyl, despropionyl *ortho*-fluorofentanyl, and *meta*-methoxy furanyl fentanyl with drift times of 4.1, 4.6, 4.5, 4.9, and 5.7 ms, respectively. These mobility spectra were obtained by running single analyte solutions prepared as described in the Methods section. The additional mobility peaks observed in the spectra are not protomers but are designated as fragments of the intact species.

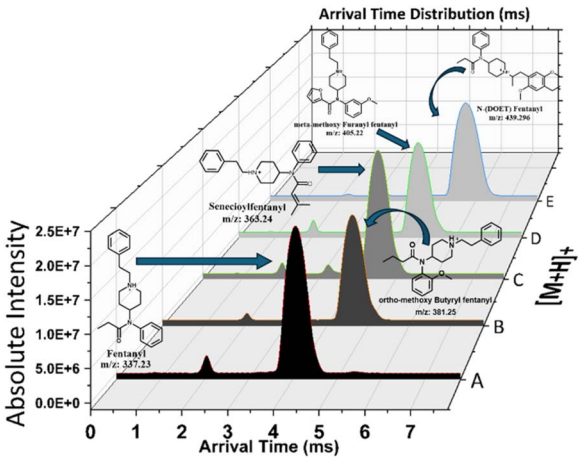

Fig. 3 Arrival time distribution spectra for 5 fentanyl analogs in nitrogen drift gas illustrating the lack of protomers in obtained mobility spectra for $[M + H]^+$ ions of (a) fentanyl (*m/z* 337), (b) *ortho*-methoxy butyryl fentanyl (*m/z* 381), (c) senecioylfentanyl (*m/z* 363), (d) *meta*-methoxy furanyl fentanyl (*m/z* 405), and (e) *N*-(DOET) fentanyl (*m/z* 43).

Protomers exist in various structural forms in the gas phase, and their appearance in spectra is not fully understood.[60,63] However, authors like Copeland *et al.* and Alderorho *et al.* suggest that the visibility and intensity of these artifacts primarily depend on the resolving power and solvent composition.[60,63] Therefore, we hypothesize that the absence of

Table 5 $^{TW}CCS_{CO_2}$, $^{TW}CCS_{N_2}$, and $^{TW}CCS_{HE}$ for 27 fentanyl analogs; isomer groups are shaded and the standard deviations (SD) for selected isomers are also provided

Compound name	Molecular formula	Exact mass	CO_2 CCS	SD	N_2 CCS	SD	He CCS	SD
N-Methyl norfentanyl	$C_{15}H_{22}N_2O$	247.18	199.69	4.06	158.78	0.31	86.68	0.17
(±)-*Cis*-3-methyl norfentanyl	$C_{15}H_{22}N_2O$	247.18	205.44		159.21		86.43	
Despropionyl *ortho*-fluorofentanyl	$C_{19}H_{23}FN_2$	299.19	219.52	2.53	172.00	1.03	100.08	0.44
Despropionyl *para*-fluorofentanyl	$C_{19}H_{23}FN_2$	299.19	223.10		173.46		99.46	
3′-Methyl fentanyl	$C_{23}H_{30}N_2O$	351.24	233.45	0.43	189.07	0.29	113.08	0.02
2′-Methyl fentanyl	$C_{23}H_{30}N_2O$	351.24	234.06		188.65		113.04	
4-Methyl fentanyl	$C_{23}H_{30}N_2O$	351.24	234.37		186.47		113.95	
Senecioylfentanyl	$C_{24}H_{30}N_2O$	363.24	237.96	1.89	192.54	1.61	113.28	0.69
Tigloyl fentanyl	$C_{24}H_{30}N_2O$	363.24	235.29		190.26		114.26	
N-(Phentermine) fentanyl	$C_{24}H_{32}N_2O$	365.26	235.07	2.79	190.64	2.72	114.87	0.44
Para-methyl butyryl fentanyl	$C_{24}H_{32}N_2O$	365.26	239.01		194.48		114.25	
Ortho-methoxy butyryl fentanyl	$C_{24}H_{32}N_2O_2$	381.25	239.07	4.27	194.33	2.65	119.33	1.57
Para-methoxy butyryl fentanyl	$C_{24}H_{32}N_2O_2$	381.25	245.12		198.08		121.55	
Ortho-fluoro valeryl fentanyl	$C_{24}H_{31}FN_2O$	383.25	239.03	2.34	193.14	1.31	119.22	0.43
Meta-fluoro valeryl fentanyl	$C_{24}H_{31}FN_2O$	383.25	242.34		195.75		119.84	
Para-chloroisobutyryl fentanyl	$C_{23}H_{29}ClN_2O$	385.20	242.78	1.06	196.10	0.37	120.03	0.86
Para-chlorobutyryl fentanyl	$C_{23}H_{29}ClN_2O$	385.20	244.28		196.62		121.24	
Meta-methyl furanyl fentanyl	$C_{25}H_{28}N_2O_2$	389.22	242.42	0.23	196.71	0.02	122.07	0.60
Para-methyl furanyl fentanyl	$C_{25}H_{28}N_2O_2$	389.22	242.75		196.69		122.91	
N-(DOM) fentanyl	$C_{26}H_{36}N_2O_3$	425.28	252.76	1.79	207.43	1.43	129.64	0.92
N-(2C-G) fentanyl	$C_{26}H_{36}N_2O_3$	425.28	252.90		205.89		127.82	
N-(2C-E) fentanyl	$C_{26}H_{36}N_2O_3$	425.28	255.92		208.74		129.02	
N-(DOET) fentanyl	$C_{27}H_{38}N_2O_3$	439.30	257.90	1.65	210.96	1.22	131.78	0.25
N-(2C-P) fentanyl	$C_{27}H_{38}N_2O_3$	439.30	258.20		213.13		131.57	
N-(2C-iP) fentanyl	$C_{27}H_{38}N_2O_3$	439.30	260.89		213.01		131.28	
N-(2C-T-7) fentanyl	$C_{27}H_{38}N_2O_3S$	471.27	266.22	0.25	217.43	0.10	138.17	0.49
N-(2C-T-4) fentanyl	$C_{27}H_{38}N_2O_3S$	471.27	266.58		217.29		129.02	

protomers in our measurements is due to the limited resolving power of the analytical method employed. Furthermore, for singly protonated $[M + H]^+$ fentanyl (*m*/*z* 337.26), two mobility peaks were observed in drift-tube studies conducted by Alderoho *et al.*, and thus two $^{DT}\Omega_{N_2}$ values were reported: 184.10 Å^2 and 189.10 Å^2.[68] The initial value (184.10 Å^2) was said to have been derived from the major mobility peak observed in their experiment, which is why we chose to compare it to our measured 183.73 Å^2 $^{TW}\Omega_{N_2}$ value, resulting in a −0.2% difference. For despropionyl *meta*-methylfentanyl a $^{DT}\Omega_{N_2}$ value of 179.4 Å^2 was reported for the major mobility peak, resulting in a 0.1% difference when compared to our measured $^{TW}\Omega_{N_2}$ value of 179.51 Å^2.[68] For (±)-*cis*-isofentanyl (*m*/*z* 337.24) we measured a single $^{TW}\Omega_{N_2}$ value of 183.51 Å^2; while Alderorho *et al.* reported a $^{DT}\Omega_{N_2}$ value of 183.70 Å^2 derived from the major mobility peak, which also results in a −0.1% difference.[68] Alderorho *et al.* also reported CCS values for the major mobility peaks of the following fentanyl analogs: *ortho*-fluorofentanyl (184.70 Å^2), *para*-methyl acetyl fentanyl (186.40 Å^2), cyclopropyl fentanyl (186.20 Å^2), isobutyryl fentanyl (187.40 Å^2), and butyryl fentanyl (188.30 Å^2), which result in differences of −0.1%, −0.2%, 0.5%, 0.3%, and −0.1%, respectively, when compared to our reported value, as illustrated in Table 4.[68]

In a separate study conducted by Lian *et al.*, only one $^{DT}\Omega_{N_2}$ value (181.40 Å^2) for fentanyl was reported, which differs by 1.3% from our measured 183.73 Å^2 $^{TW}\Omega_{N_2}$ value.[69] Another study by Butler *et al.* also reported two $^{DT}CCS_{N_2}$ for fentanyl, 181.70 Å^2 and 187.90 Å^2.[70] Out of these two values, they reported 181.70 Å^2 as having been derived from the major mobility peak, and when compared to our value it differed by 1.1%.[70] The studies conducted by Alderoho *et al.*, Lian *et al.*, and Butler *et al.* all used single-field methods to measure CCS values on a 6560 IM-QTOF instrument.[68–70] Out of all the compounds analyzed by Lian *et al.* and Butler *et al.* only one was from the fentanyl [*m*/*z* 337.22] class while the rest were from different drug classes.[68–70] Only Alderoho *et al.* analyzed several compounds belonging to the fentanyl chemical class.[68] This means that the instrument parameters used in Alderoho *et al.*'s study were fine tuned for fentanyl analogs and did not need to be broadened for varying drug classes and masses; thus we conclude that their values are the most accurate out of the three studies.

Due to the novelty of TWIM mass spectrometry, there are limited ^{TW}CCS data available for fentanyl analogs. To the best of our knowledge a paper written by Hollerbach *et al.* is the only publication reporting $^{TW}CCS_{N_2}$ values for 9 fentanyl analogs using dual-gated SLIM Orbitrap technology.[61] And only 2 out of those fentanyl compounds were analyzed in this study: fentanyl (*m*/*z* 337.26) and *para*-chloroisobutyryl fentanyl (*m*/*z* 385.20). The $^{TW}CCS_{N_2}$ value for fentanyl $[M + H]^+$ reported by Hollerbach *et al.* was 182.01 Å^2, which differs by 0.9% from our reported value. Hollerbach *et al.* also reported a $^{TW}CC_{N_2}$ value of 194.57 Å^2 for *para*-chloroisobutyryl fentanyl $[M + H]^+$, while we report a value of 196.10 Å^2, resulting in a 0.8% difference.[61] The rest of the fentanyl analogs analyzed in that study were not used in our study and therefore cannot be commented on.

3.3 Mobility separation of isomers

Among the 110 fentanyl analogs analyzed, 60 exhibited isomers, while only 11 of the 16 non-fentanyl opioids showed isomeric forms. Notably, no isomers were observed within the fentanyl-related compounds. The measured Ω_{N_2}, Ω_{He}, and Ω_{CO_2} values and associated standard deviations (SD) for 27 fentanyl isomers are reported in Table 5. For the complete list of isomers, please refer to Table S.8 of the ESI.† The $^{TW}CCS_{N_2}$ values for *N*-methyl norfentanyl and (±)-*cis*-3-methyl norfentanyl are 158.78 Å^2 and 159.21 Å^2, respectively. These values differ by 0.43 Å^2 while $^{TW}CCS_{He}$ values, 86.68 Å^2 and 86.43 Å^2, differ by only 0.25 Å^2 and

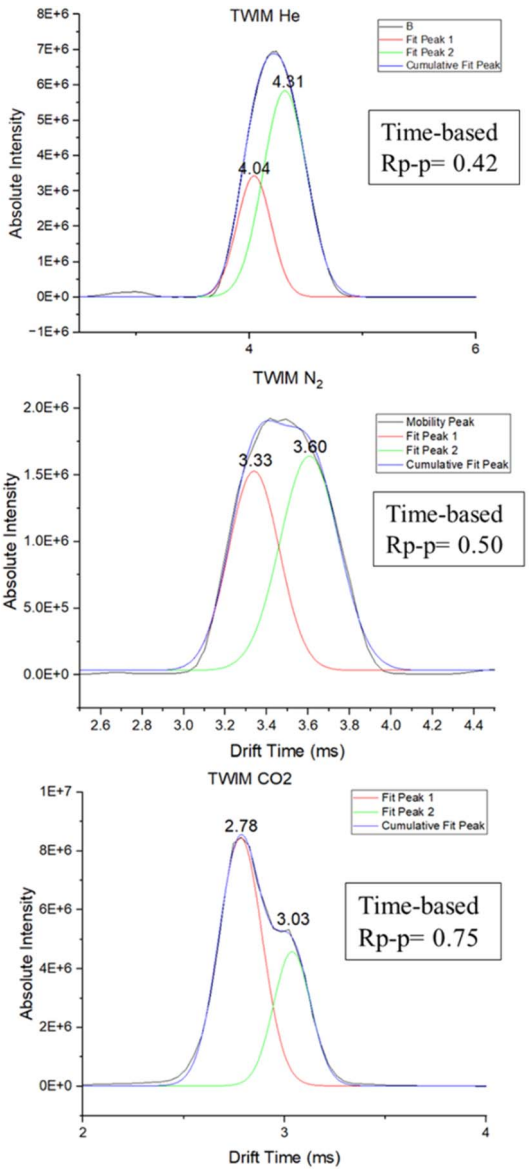

Fig. 4 Arrival time spectra for despropionyl *para*-fluorofentanyl and despropionyl *ortho*-fluorofentanyl in helium drift gas (top), nitrogen (middle), and carbon dioxide (bottom). Gaussian peak fitting was performed to determine the peak-to-peak resolving power (R_{p-p}) for each drift gas. The calculated R_{p-p} values were 0.42 for He, 0.50 for N_2, and 0.75 for CO_2.

$^{TW}CCS_{CO_2}$ values, 199.69 Å^2 and 205.44 Å^2, differ by 5.75 Å^2. The majority of the fentanyl analog isomers follow this trend, where the CCS% difference increases when using CO_2, followed by N_2 and He, as expected. Therefore, when CO_2 is used as the buffer gas, several fentanyl isomers are clearly distinguishable, whereas under He and N_2 conditions, their IM separation is significantly reduced for the majority. Thus, CO_2 as the IM buffer gas generally extends the drift time profile, leading to improved separation, as seen in Fig. 4, which illustrates the arrival time spectra for despropionyl *para*-fluorofentanyl and despropionyl *ortho*-fluorofentanyl in helium, nitrogen, and carbon dioxide drift gases. Yet despite the high sensitivity of the instrument and the optimal reproducibility between CCS measurements, as seen in Fig. 4, mobility separation of isomers was generally poor in mixtures due to the low resolving power $\approx\leq 10$ $\Omega/\Delta\Omega$ (FWHM). This is in part due to the method developed to encompass a wide range of m/z ions. A method that allows only certain points can increase resolving power but this was outside the scope of this paper.

3.4 Comparison of theoretical and experimentally derived N_2, He, and CO_2 CCS values

Computationally derived collision cross sections (CCS) for each fentanyl analog were calculated using MobCross, which employs the projection approximation.[66] The process involves rotating the drawn molecule (neutral singlets in this study) 2000 times within a circle, with its radius based on the distance from the center-of-mass. During each rotation, 5000 random buffer gas species are placed, and interactions with the molecular ion are recorded as hits or misses. The hit ratio is multiplied by the circle's area (πr^2) and averaged across all projections to determine the cross-sectional area. Molecular coordinates are converted to a center-of-mass system, and rotations are performed about the center. Using the quaternion algorithm accelerates the simulations, enabling faster calculations for molecules under 10 000 Da, completing in under 5 minutes compared to longer times with Eulerian angles. Generated theoretical (Ω_{N_2}) values were plotted against the measured values ($^{TW}\Omega_{N_2}$), as shown in Fig. 5. The results demonstrate an excellent linear correlation, with an R^2 value of 0.9564. The values used to construct this graph, along with the corresponding percentage differences ΔCCS%, are reported in Table S.9 of the ESI.† Although there is an excellent correlation between these values, our computational approach requires further refinement, as experimental and computational values vary significantly (±0.1–15.0 ΔCCS%). The majority of the MobCross values differed by more than ±3%, with only 23 compounds exhibiting a percentage difference lower than <±3%. Our data indicate that as the mass of the analytes increases, the percentage difference in their measured values also increases. This discrepancy can be attributed to the influence of protonation states, which were not initially accounted for in the analysis, since we used neutral singlets of the relevant molecules. Protonation significantly alters the collision cross-section (CCS) of an analyte; our goal was to assess whether using a neutral structure, followed by a correction factor to account for the $[M + H]^+$ protonation state, could yield accurate CCS values. Since various charge carriers are employed during analysis, obtaining neutral CCS values is essential for establishing a baseline measurement for all types of protonation. Once this baseline is determined, a charge carrier-specific correction factor can be applied to refine the results. Our findings suggest that additional computational work is necessary to achieve consistent accuracy. We recommend considering both protonation states of fentanyl and employing multiple charge carriers to determine the corresponding CCS values, as protonation will also alter the equilibrium geometry slightly which may contribute to the percent errors observed in the data compared to the experimental data. This approach would facilitate the development of a more precise correction factor, leading to improved accuracy in CCS measurements.

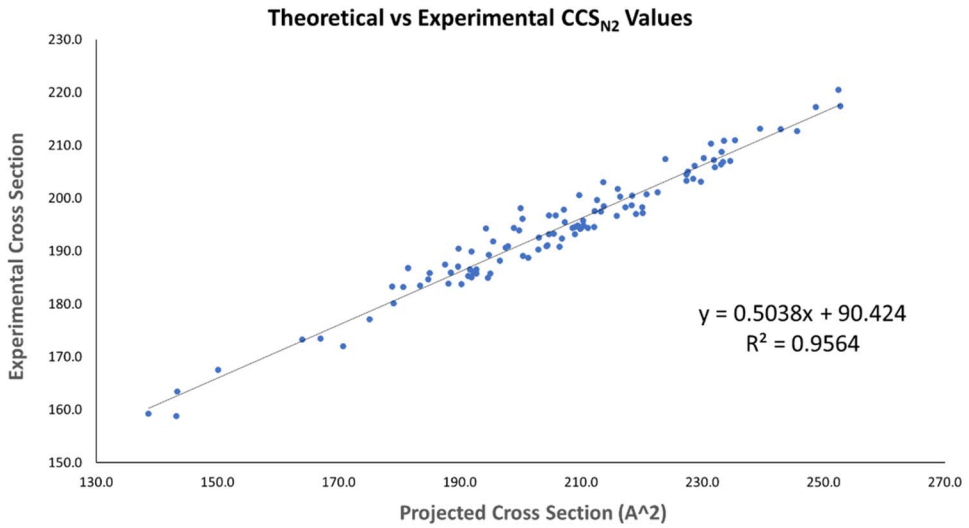

Fig. 5 Plot of the calculated Collision Cross Sections (CCS) in N_2 gas against experimental values obtained in N_2 gas.

4. Conclusion

In this study, we measured the $^{TW}CCS_{N_2}$, $^{TW}CCS_{He}$, and $^{TW}CCS_{CO_2}$ values for precursor ions $[M + H]^+$ of 110 fentanyl analogs, 7 fentanyl-related compounds, and 31 synthetic opioids using the Synapt G2-Si by Waters. To the best of our knowledge, here we report the first ^{TW}CCS database for more than 100 fentanyl analogs analyzed in positive ion mode, using three independently implemented drift gases (N_2, He, and CO_2). We present this database with the hope that it will serve as a useful reference for any individual wishing to characterize known or unknown fentanyl analogs. Interday measurements showed high reproducibility, with deviations as low as 0.18 RSD%. Our reported Ω_{N_2} values are highly consistent with previously published DTIM values with differences typically around ±0.1%, suggesting a high degree of accuracy for the obtained CCS values. We also present theoretical data that can be used to predict the CCS value of an unknown opioid. Experimental and theoretical values differed by 0.1–15%, and thus computational refinement is required. Our ^{TW}CCS database can be used to improve the accuracy and precision of analysis, thus increasing confidence in fentanyl characterization compared to traditional analytical approaches. We attribute the small, but measurable differences in mobility between fentanyl analog isomers to short-range van der Waals interaction between the ion and neutral gas molecules, while the large mobility differences between analogs are due to long-range charge induced dipole interactions caused by differences in gas polarizability. The CCS difference between positional isomers was too small to be distinguished by the method employed, but isobaric separation was achievable. Lastly, although it has been proven that TWIM CCS measurement accuracy increases when molecules from the same class as the analyte are used as calibrants, in this study we demonstrate that the Major Mix (Waters) calibration solution is sufficient for precise and accurate CCS measurements of synthetic opioids.

Data availability

The data supporting this article have been included as part of the ESI.†

Author contributions

G. F. Verbeck: funding acquisition and project administration. T. D. Golden: project administration. K. A. Reyes Monoy: conceptualization, methodology, investigation, validation, data curation, formal analysis, visualization, project administration, writing – original draft, writing – review & editing. D. Perez: data curation. L. NgoC: data curation. R. Demmelash: data curation. A. Mancilla: data curation. H. Castro: data curation. N. R. Wiese: formal analysis and data curation, W. A. Murillo: formal analysis and data curation.

Conflicts of interest

There is no conflict of interest for the data presented in this manuscript.

Acknowledgements

TRACEABLE OPIOID MATERIAL, TOM KITS, and the TOM KITS logo are marks of the US Department of Health and Human Services. The authors would like to acknowledge the CDC contractor, Cayman Chemical Company, for the manufacturing, distribution, and customer support of the FAS Kit.

References

1 T. H. Stanley, The Fentanyl Story, *J. Pain*, 2014, **15**, 1215–1226.
2 T. H. Stanley, Fentanyl, *J. Pain Symptom Manage.*, 2005, **29**, 67–71.
3 S. H. Hassanien, J. R. Bassman, C. M. Perrien Naccarato, *et al.*, In vitro pharmacology of fentanyl analogs at the human mu opioid receptor and their spectroscopic analysis, *Drug Test. Anal.*, 2020, **12**, 1212–1221.
4 R. S. Vardanyan and V. J. Hruby, Fentanyl-Related Compounds and Derivatives: Current Status and Future Prospects for Pharmaceutical Applications, *Future Med. Chem.*, 2014, **6**, 385–412.
5 Drug Enforcement Agency, *DEA Warns of Increase in Mass-Overdose Events Involving Deadly Fentanyl*, **https://www.dea.gov/press-releases/2022/04/06/dea-warns-increase-mass-overdose-events-involving-deadly-fentanyl**, accessed August 2024.
6 J. Lemahieu, A. Me and P. Davis, et al. An expanding synthetic drugs market – implications for precursor control, In *Global SMART Update*, ed. J. Gibbons, United Nations Office on Drugs and Crime, 2019, vol. 23, pp. 7–10.
7 UNODC, *World Drug Report*, United Nations Office on Drugs and Crime, 2023, pp. 44–50.
8 M. E. Rose, Are Prescription Opioids Driving the Opioid Crisis? Assumptions vs. Facts, *Pain Med.*, 2017, **19**, 793.
9 A. Thumma, K. Mfoafo, N. Babanejad, *et al.*, Abuse potential of fentanyl and fentanyl analogues, *BioImpacts*, 2024, **14**, 27691.
10 S. D. Comer and C. M. Cahill, Fentanyl: Receptor pharmacology, abuse potential, and implications for treatment, *Neurosci. Biobehav. Rev.*, 2018, **106**, 49–57.
11 J. Patocka, W. Wu, P. Oleksak, *et al.*, Fentanyl and its derivatives: pain-killers or man-killers?, *Heliyon*, 2024, **10**, e28795.
12 C. R. Breyer, D. C. Reeves, P. K. Cushwa, *et al.*, *Fentanyl and Fentanyl Analogues-Federal Trends and Trafficking Patterns*, United States Sentencing Commission, 2021.
13 J. P. Caulkins, P. C. Schicker, H. B. Milward, *et al.*, A detailed study of a prominent dark web fentanyl trafficking organization, *Global Crime*, 2024, **25**, 50–71.
14 V. W. Weedn, M. E. Zaney, B. McCord, *et al.*, Fentanyl-related substance scheduling as an effective drug control strategy, *J. Forensic Sci.*, 2021, **66**, 1186–1200.
15 Z. Dai, M. A. Abate, G. S. Smith, *et al.*, Fentanyl and fentanyl-analog involvement in drug-related deaths, *Drug Alcohol Depend.*, 2019, **196**, 1–8.

16 J. P. Caulkins and K. Humphreys, *New Drugs, Old Misery: The Challenge of Fentanyl, Meth, and Other Synthetic Drugs*, The Manhattan Institute, 2023.
17 N. Lassi, Strengthening pill press control to combat fentanyl: legislative and law enforcement imperatives, *Exploratory Research in Clinical and Social Pharmacy*, 2023, **11**, 100321.
18 M. L. Jewell, H. L. Jewell, R. Singer, *et al.*, Patient Safety Advisory: Fentanyl Counterfeit Prescription Medications that Contain Fentanyl and Patient Safety, *Aesthetic Plast. Surg.*, 2023, **47**, 1234–1238.
19 E. Harris, US Deaths From Overdoses Involving Fake Pills Have Increased, *JAMA, J. Am. Med. Assoc.*, 2023, **330**, 1217.
20 T. DeAngelo, Fake Pharmaceuticals, in *Trends in Counterfeit Drugs*, ed. K.M. Elkins, CRC Press, Boca Raton, 1st edn, 2024, pp. 51–62.
21 H. Fallang, History and Overview of Counterfeit Drugs Cases, in *Trends in Counterfeit Drugs*, ed. K. M. Elkins, CRC Press, Boca Raton, 1st edn, 2023, pp. 10–16.
22 C. F. Ramos-Matos, K. G. Bistas and W. Lopez-Ojeda, *Fentanyl*, StatPearls Publishing, Treasure Island, FL, January 2025, PMID: 29083586.
23 J. J. Palamar, D. Ciccarone, C. Rutherford, *et al.*, Trends in seizures of powders and pills containing illicit fentanyl in the United States, 2018 through 2021, *Drug Alcohol Depend.*, 2022, **234**, 109398.
24 M. H. Baumann, G. Tocco, D. M. Papsun, *et al.*, U-47700 and Its Analogs: Non-Fentanyl Synthetic Opioids Impacting the Recreational Drug Market, *Brain Sci.*, 2020, **10**, 895.
25 DEA Special Testing and Research Laboratory (SFL1) of the Office of Forensic Sciences, Drug Enforcement Administration Fentanyl Profiling Program Report First Half CY 2021, Drug Enforcement Administration, 2022.
26 P. F. J. Lipiński and J. Matalińska, Fentanyl Structure as a Scaffold for Opioid/Non-Opioid Multitarget Analgesics, *Int. J. Mol. Sci.*, 2022, **23**, 2766.
27 B. Westhoff, *Fentanyl, Inc.: How Rogue Chemists Are Creating the Deadliest Wave of the Opioid Epidemic*, Atlantic Monthly Press, 2019.
28 L. M. Eubanks, t. Pholcharee, D. Oyen, *et al.*, An Engineered Human-Antibody Fragment with Fentanyl Pan-Specificity That Reverses Carfentanil-Induced Respiratory Depression, *ACS Chem. Neurosci.*, 2023, **14**, 2849–2856.
29 K. M. Elkins, Results from a Survey of Trends in Seized Counterfeit Drugs, in *Trends in Counterfeit Drugs*, ed. K. M. Elkins, CRC Press, Boca Raton, 1st edn, 2023, pp. 63–75.
30 Scientific Working Group for Forensic Toxicology, Scientific Working Group for Forensic Toxicology (SWGTOX) Standard Practices for Method Validation in Forensic Toxicology, *J. Anal. Toxicol.*, 2013, **37**, 452–474.
31 Federal Bureau of Investigation Scientific Working Group for the Analysis of Seied Drugs, Forensic Science Communications, 2005, vol. 7, **https://archives.fbi.gov/archives/about-us/lab/forensic-science-communications/fsc/jan2005/standards/2005standards11.htm**.
32 S. A. Schleman, M. Gomez, S. Sukumaran, *et al.*, Distinguishing isomers of fentanyl analogs using FT-Raman, in *Thermo Scientific Report*, 2018, pp. 1–2.
33 Z. Lian, C. Lu, Q. Sun, *et al.*, A nonmetal substrate of surface-enhanced Raman spectroscopy for trace fentanyl detection, *J. Raman Spectrosc.*, 2023, **54**, 580–586.
34 Q. Nan, W. Hejian, X. Ping, *et al.*, Investigation of Fragmentation Pathways of Fentanyl Analogues and Novel Synthetic Opioids by Electron Ionization High-Resolution Mass Spectrometry and Electrospray Ionization High-Resolution Tandem Mass Spectrometry, *J. Am. Soc. Mass Spectrom.*, 2020, **31**, 277–291.
35 H. G. Pierzynski, L. Neubauer and C. Choi, *Tips for Interpreting GC-MS Fragmentation of Unknown*, Cayman Chemicals, 2017.
36 FDA, *Development of New Stereoisomeric Drugs*, Center for Drug Evaluation and Research, 1992.
37 V. Velagapudi and R. Sethi, Illicit Non-Pharmaceutical Fentanyl and its Analogs: A Short Review of Literature, *Kjm*, 2023, **16**, 25–27.
38 A. J. Kearsley and A. S. Moorthy, *Identifying fentanyl with mass spectral libraries*, National Institute of Standards and Technology, 2021, DOI: **10.26434/chemrxiv.14176952.v1**.
39 Q. Nan, W. Hejian, X. Ping, *et al.*, Investigation of Fragmentation Pathways of Fentanyl Analogues and Novel Synthetic Opioids by Electron Ionization High-Resolution Mass Spectrometry and Electrospray Ionization High-Resolution Tandem Mass Spectrometry, *J. Am. Soc. Mass Spectrom.*, 2020, **31**, 277–291.
40 C. A. Valdez, R. N. Leif, R. D. Sanner, *et al.*, Structural modification of fentanyls for their retrospective identification by gas chromatographic analysis using chloroformate chemistry, *Sci. Rep.*, 2021, **11**, 22489.
41 A. S. Moorthy, E. P. Erisman, A. J. Kearsley, *et al.*, On the challenge of unambiguous identification of fentanyl analogs: exploring measurement diversity using standard reference mass spectral libraries, *J. Forensic Sci.*, 2023, **68**, 1494–1503.
42 J. T. Davidson, Z. J. Sasiene and G. P. Jackson, The influence of chemical modifications on the fragmentation behavior of fentanyl and fentanyl-related compounds in electrospray ionization tandem mass spectrometry, *Drug Test. Anal.*, 2020, **12**, 957–967.
43 Y. Fan, X. Lin, X. Chen, *et al.*, Application of mass spectrometry fragmentation patterns for rapid screening and structure identification of fentanyl analogues in suspicious powder, *Forensic Chem.*, 2023, **33**, 100485.
44 E. H. Denis, J. L. Bade, R. S. Renslow, *et al.*, Proton Affinity Values of Fentanyl and Fentanyl Analogues Pertinent to Ambient Ionization and Detection, *J. Am. Soc. Mass Spectrom.*, 2022, **33**, 482–484.
45 Y. Zhang, J. C. Halifax, C. Tangsombatvisit, *et al.*, Development and application of a high-resolution mass spectrometry method for the detection of fentanyl analogs in urine and serum, *J. Mass Spectrom. Adv. Clin. Lab*, 2022, **26**, 1–6.
46 E. N. Shoff, M. E. Zaney, J. H. Kahl, G. W. Hime and D. M. Boland, Qualitative Identification of Fentanyl Analogs and Other Opioids in Postmortem Cases by UHPLC-Ion Trap-MSn, *J. Anal. Toxicol.*, 2017, **41**, 484.

47 J. T. Davidson, Z. J. Sasiene and G. P. Jackson, The characterization of isobaric product ions of fentanyl using multi-stage mass spectrometry, high-resolution mass spectrometry and isotopic labeling, *Drug Test. Anal.*, 2020, **12**, 496–503.
48 United Nations Office on Drugs and Crime, *Recommended Methods for the Identification and Analysis of Fentanyl and its Analogues in Biological Specimens*, United Nations Publications, United States, ST/NAR/53, 2018.
49 A. Salomone, D. Di Corcia, P. Negri, *et al.*, Targeted and untargeted detection of fentanyl analogues and their metabolites in hair by means of UHPLC-QTOF-HRMS, *Anal. Bioanal. Chem.*, 2021, **413**, 225–233.
50 D. H. Ross and L. Xu, Determination of drugs and drug metabolites by ion mobility-mass spectrometry: a review, *Anal. Chim. Acta*, 2021, **1154**, 338270.
51 K. M. Hines, D. H. Ross, K. L. Davidson, *et al.*, Large-Scale Structural Characterization of Drug and Drug-Like Compounds by High-Throughput Ion Mobility-Mass Spectrometry, *Anal. Chem.*, 2017, **89**, 9023–9030.
52 K. Richardson, D. Langridge and K. Giles, Fundamentals of travelling wave ion mobility revisited: I. Smoothly moving waves, *Int. J. Mass Spectrom.*, 2018, **428**, 71–80.
53 S. M. Stow, T. J. Causon, X. Zheng, *et al.*, An Interlaboratory Evaluation of Drift Tube Ion Mobility-Mass Spectrometry Collision Cross Section Measurements, *Anal. Chem.*, 2017, **89**, 9048–9055.
54 J. W. Lee, K. L. Davidson, M. F. Bush, *et al.*, Collision cross sections and ion structures: development of a general calculation method via high-quality ion mobility measurements and theoretical modeling, *Analyst*, 2017, **142**, 4289.
55 C. N. Naylor, T. Reinecke and B. H. Clowers, Assessing the Impact of Drift Gas Polarizability in Polyatomic Ion Mobility Experiments, *Anal. Chem.*, 2020, **92**, 4226.
56 Y. Simón-Manso, Ion-Neutral Collision Cross Section as a Function of the Static Dipole Polarizability and the Ionization Energy of the Ion, *J. Phys. Chem. A*, 2023, **127**, 3274.
57 K. Richardson, d. Langridge, S. M. Dixit, *et al.*, An Improved Calibration Approach for Traveling Wave Ion Mobility Spectrometry: Robust, High-Precision Collision Cross Sections, *Anal. Chem.*, 2021, **93**, 3542–3550.
58 S. M. Dixit and B. T. Ruotolo, A Semi-Empirical Framework for Interpreting Traveling Wave Ion Mobility Arrival Time Distributions, *J. Am. Soc. Mass Spectrom.*, 2019, **30**, 956–966.
59 D. N. Mortensen, A. C. Susa and E. R Williams, Collisional Cross-Sections with T-Wave Ion Mobility Spectrometry without Experimental Calibration, *J. Am. Soc. Mass Spectrom.*, 2017, **28**, 1282–1292.
60 R. Aderorho and C. D. Chouinard, Determining protonation site in fentanyl protomers using ion mobility-aligned MS/MS fragmentation, *Int. J. Mass Spectrom.*, 2024, **496**, 117185.
61 A. L. Hollerbach, Y. M. Ibrahim, V. Meras, *et al.*, A Dual-Gated Structures for Lossless Ion Manipulations-Ion Mobility Orbitrap Mass Spectrometry Platform for Combined Ultra-High-Resolution Molecular Analysis, *Anal. Chem.*, 2023, **95**, 9531–9538.
62 R. Aderorho and C. D. Chouinard, Improved separation of fentanyl isomers using metal cation adducts and high-resolution ion mobility-mass spectrometry, *Drug Test. Anal.*, 2024, **16**, 369–379.
63 C. R. Johnson, H. M. Sabatini, R. Aderorho, *et al.*, Dependency of fentanyl analogue protomer ratios on solvent conditions as measured by ion mobility-mass spectrometry, *J. Mass Spectrom.*, 2024, **59**, e5070.
64 A. R. Forero, T. L. Valadares, M. Willetts, *et al.*, Fentanyl Analog Screening using LC-TIMS-TOF MS/MS, *J. Visualized Exp.*, 2024, 213–215.
65 J. C. May, C. B. Morris and J. A. McLean, Ion Mobility Collision Cross Section Compendium, *Anal. Chem.*, 2017, **89**, 1032–1044.
66 F. G. Verbeck, *Development of a Variable-Temperature Ion Mobility/Time-of-Flight Mass Spectrometer for Separation of Electronic Isomers*, Texas A&M University, 2005, pp. 45–53.
67 M. F. Bush, I. D. G. Campuzano and C. V. Robinson, Ion Mobility Mass Spectrometry of Peptide Ions: Effects of Drift Gas and Calibration Strategies, *Anal. Chem.*, 2012, **84**, 7124–7130.
68 R. Aderorh and C. D Chouinard, Improved separation of fentanyl isomers using metal cation adducts and high-resolution ion mobility-mass spectrometry, *Drug Test. Anal.*, 2024, **16**, 369–379.
69 R. Lian, F. Zhang, Y. Zhang, *et al.*, Ion mobility derived collision cross section as an additional measure to support the rapid analysis of abused drugs and toxic compounds using electrospray ion mobility time-of-flight mass spectrometry, *Anal. Methods*, 2018, **1**, 749–756.
70 K. E. Butler and E. S. Baker, A High-Throughput Ion Mobility Spectrometry-Mass Spectrometry Screening Method for Opioid Profiling, *J. Am. Soc. Mass Spectrom.*, 2022, **33**, 1904–1913.